Reactive & Functional Polymers 73 (2013) 1306–1318

Contents lists available at SciVerse ScienceDirect

Reactive & Functional Polymers

journal homepage: www.elsevier.com/locate/react

Mechanical and rheological behavior of pNIPAAM crosslinked macrohydrogel

G.L. Puleo [a,1], F. Zulli [c,1], M. Piovanelli [a,b,1], M. Giordano [c], B. Mazzolai [a], L. Beccai [a,*], L. Andreozzi [c]

[a] Center for Micro-BioRobotics@SSSA, Istituto Italiano di Tecnologia (IIT), 56025 Pontedera, Pisa, Italy
[b] The BioRobotics Institute, Scuola Superiore Sant'Anna, 56025 Pontedera, Pisa, Italy
[c] Department of Physics "E. Fermi", University of Pisa and IPCF-CNR, 56127 Pisa, Italy

ARTICLE INFO

Article history:
Received 1 March 2013
Received in revised form 1 July 2013
Accepted 3 July 2013
Available online 11 July 2013

Keywords:
Macrohydrogel
N-isopropylacrylamide
Shear rheology
Mechanical properties
Hydrogel model

ABSTRACT

In this study for the first time we investigate the most common reticulated N-isopropylacrylamide (pNIPAAM) macrohydrogel for both its mechanical response and shear rheological behavior in time and frequency domains. Hydrogels are characterized by water content volume and weight measurements, FT-IR spectroscopy, scanning electron microscopy and reflecting index. Compressive uniaxial tests on equilibrated hydrogels individuate a hookean response within a 30% strain range with E_c modulus of 12.2 kPa, and a neo-hookean response within a 79% strain range which upper limit corresponds to material rupture with G_c modulus of 3.8 kPa. Tensile experiments performed for the first time on the pure material evidence a rupture limit for a strain around 30% with hookean modulus E_t of 24.8 kPa and neo-hookean modulus G_t of 7.3 kPa. Rheological studies, carried out in linear response regime around the hydrogel swelling–deswelling transition, report relaxation times of the kinetics towards the equilibrium at different temperatures. The phase transition of pNIPAAM is monitored and the transition temperature is determined following the temperature dependence of the shear modulus. We apply different literature models to the rheological response and to the swelling–deswelling transition of the hydrogel. Finally, we analyze the results providing values for microscopic material parameters such as crosslink density and mesh size.

1. Introduction

1.1. Hydrogel material structure

Hydrogels are hydrophilic polymeric materials not soluble in water, able to swell during an impressive water or physiological fluids uptake (up to 99.9% of their swelled weight) [1]. This definition also includes a wide range of natural materials of both plant and animal origin, synthetic polymeric materials and bio-hybrid materials. Natural sources derived hydrogels were formed starting from collagen, the main protein of mammalian extracellular matrix, from hyaluronic acid (HA), ubiquitous polysaccharides, or from alginate, agarose, and chitosan, polysaccharides produced by marine algae or crustaceous [2]. Neutral synthetic hydrogel were generated from derivatives of poly(hydroxyethyl methacrylate) (PHEMA), poly-(ethylene glycol) (PEG), and poly(vinyl alcohol) (PVA) [2]. By integrating biological entities with synthetic hydrogels, indeed, novel systems were created, displaying enhanced cellular adhesion or supporting enzymatic activity [2,3].

Since the introduction of hydrogels as soft contact lenses in the 1960s [4] their use has increased tremendously and nowadays they are favored in a broad range of pharmaceutical and biomedical applications: they are applied for tissue engineering as space filling agents and as three-dimensional structures that organize cells and present stimuli to direct the formation of a desired tissue [2]. In drug delivery system they are used as drug carriers able to control drug release [5]. More challenging uses of these kinds of materials originated in the last decades and are mainly related to physical and chemical sensing, and smart actuation, in response to conditions in the environment thus re-focusing research attention on their peculiar material properties [6,7].

An hydrogel chemical structure strongly influences its physical properties: the dried equivalent of hydrogel, called xerogel, is, from a structural point of view, an homopolymer or a copolymer network held together by means of chemical crosslinks (like covalent bonds in permanent hydrogel) or physical junctions (e.g. secondary forces, crystallite formation, chain entanglements like in physical hydrogel) [8]. The water holding capacity of a xerogel (and the final water uptake of the corresponding hydrogel) is dependent on the

* Corresponding author. Tel.: +39 050883079; fax: +39 050883402.
E-mail address: lucia.beccai@iit.it (L. Beccai).
[1] These authors contributed equally to this work.

1381-5148/$ - see front matter © 2013 Elsevier Ltd. All rights reserved.
http://dx.doi.org/10.1016/j.reactfunctpolym.2013.07.004

number of hydrophilic groups and the crosslink density in the network. The higher the number of the hydrophilic groups, the higher the capacity to hold water, while with an increase in the crosslink density there is a decrease in the equilibrium swelling due to the reduction of mobility of available hydrophilic groups. As the crosslink density increases, there is a subsequent increase in the hydrophobicity and a corresponding decrease in the stretchability of the polymer network [8].

The nature of monomer and crosslinker also leads to interesting new properties of hydrogels [8]: the swelling equilibrium can be stable in different environmental conditions, i.e. it is not affected by variations of pH, temperature or electric field. In this case, the properties of swelling depend just on the fixed interaction between water and polymer network (conventional hydrogel). Conversely hydrogel hydration can be influenced by pH, electric field, temperature, inducing different water uptake in parts of the polymer network subject to different conditions (stimuli responsive hydrogel). This second class of hydrogels attracted widespread interest in the last decade [8].

1.2. Importance of pNIPAAM hydrogel

Among stimuli responsive hydrogels, pNIPAAM hydrogels showed very interesting properties. Poly(*N*-isopropylacrylamide) (pNIPAAM) hydrogel is a homopolymer network obtained by controlled polymerization of N-isopropylacrilamide monomers and crosslinked by MBAAM [9]. The polymerization mechanism is normally radical and a wide range of initiators are classically used for this reaction (APS, APS + TEMED, AIBN, Calcon™ dye...). pNIPAAM and its copolymers exhibit thermo-responsivity because of their strong volume dependence in response to a change in surrounding temperature with respect to certain value, called the lower critical solution temperature (LCST). When temperature is below the LCST value the xerogel is in hydrogel form, swollen and hydrophilic; while, when temperature is above the LCST value, the hydrogel shrinks and turns into a collapsed and hydrophobic state expelling water [9]. This special behavior is due to the presence of both hydrophilic amide groups and hydrophobic isopropyl groups in its side-chains [9]. Due to these dramatic thermo-responsive properties, pNIPAAM hydrogels have attracted great interest for a wide variety of applications, including controlled drug delivery, immobilization of enzymes, separation of proteins and recyclable absorbents, and so on [10].

1.3. Previous mechanical characterization

Despite their ubiquitous uses, a full study of both the mechanical response and rheological behavior of pNIPAAM crosslinked hydrogels is still missing. To our knowledge, until today the majority of studies on mechanical characterization were related to microgel/solvent dispersions [11], pNIPAAM xerogel [12] rather than to crosslinked pNIPAAM hydrogel [13]. Moreover, even if APS/TEMED or simply APS under nitrogen atmosphere were the synthesis methods mostly used, nearly all characterization work was devoted to other kinds of synthetic processes. Several authors ascribed the lack of information to difficulties in clamping the hydrogel in order to retrieve the mechanical properties [14]. Main achievements reported in literature regard measurements ofcontact angle and Young modulus. Contact angle studies, reported by Zhang et al. [15], underlined the strong dependence of this parameter from temperature: pNIPAAM hydrogel presents a contact angle around 63.5° under the LCST transition and 93.2° above this temperature [15]; this behavior is explained by the rearrangement of pNIPAAM polymer in a secondary structure containing NH-carbonyl hydrogen bonds [16]. The Young modulus obtained under compression was firstly reported by Gundogan et al. in 2002 [17], in a work about pNIPAAM gel functionalized with ionic groups: they obtained a value of 5.63 kPa in presence of 1.2 mol% of crosslinker. The only partial information about tensile modulus of pure pNIPAAM with the samecrosslinker percentage was indirectly derived from studies on latex/pNIPAAM composite and is affected by the significant polyester influence on the mixture mechanical properties [18]. Matzelle et al. proposed in 2003 the scan force microscopy (SFM) as a new technique for the study of pNIPAAM hydrogel, obtaining a *G* modulus between 5 and 10 kPa [19]. Finally, the dynamic mechanical analysis (DMA) with parallel plates resulted in a static modulus that is varying from 20 to 120 kPa in response to a 0–1000 mN stress range [20]. A dynamic rheological characterization on the bulk macrohydrogel has very recently appeared in the literature [21], but when we started our work just a rheology approach tohydrogel micro-dispersion in water solution was reported [22–25].

1.4. Aim of the work

Considering the importance of pNIPAAM hydrogel in material chemistry for its tissue-like elasticity, its ability to transport nutrients and waste, its use as efficient and controllable drug-carrier [26] and its recent re-discovery for smart actuation [27], our attention was focused on studying the mechanical properties of this kind of hydrogel with special attention to the dynamic viscoelastic and static elastic behavior. Therefore we addressed a thorough characterization of the material by means of uniaxial compression and tensile tests, and rheological measurements. To this purpose the most used synthesis, like the one promoted by APS, was chosen and the most common quantity of crosslinker was used (1.2 mol%). Experimental measurements were repeated in order to obtain a complete characterization of the synthesized material and an accuratereproducibility of data. Simple thermodynamic models were used to understand experimental results and to pursue the physical correlation between mechanical behavior and chemical structure. We used rheology to monitor the swelling–deswelling transition and to accomplish microscopic characterization in bulk hydrogel, in order to obtain relaxation times and material microscopic parameters starting from statistical models available in literature [28].

2. Experimental

2.1. Materials

N-isopropylacrilamide (NIPAAM) purchased by Sigma–Aldrich was recrystallized in n-hexane, recovered by filtration on paper filter and dried under vacuum. N,N,methylenebis(acrylamide) (MBAAM) and ammonium persulfate (APS) were used as supplied by Sigma–Aldrich.

2.2. Hydrogel synthesis

In a typical experiment 3 g of NIPAAM and 45 mg of MBAAM (0.29 mmol, 1.2 mol%) as a crosslinker were dissolved in 120 ml of water in a glove box under nitrogen atmosphere and degassed [6]. APS water solution (5% in water, 0.45 ml) was added and the polymerization was left under nitrogen atmosphere for 24 h at 20 °C. The gel was carefully immersed into Millipore purified water to wash out excess monomers and residual chemicals.

2.3. Water absorption

The xerogel was obtained by drying the hydrogel in the air for 2 days at room temperature and subsequently at 70 °C for

30 min. The obtained xerogel was then weighted and the volume was estimated by using a calibrated digital compass (TESA IP 67 Caliper, resolution 0.01 mm) by following a modified procedure from [18]. Afterwards, each sample was placed in an excess of water at room temperature (20 ± 0.5 °C). To reach swelling equilibrium, the hydrogels were immersed in water for at least 2 days, replacing the water every day. The swelling equilibrium was tested by measuring the volume of the gel samples. To achieve good precision, three measurements were carried out on samples of different length taken from the same gel. Then the volume fraction of the xerogel, ϕ_x (xerogel volume/volume of the hydrogel after swelling), was determined. In the same way the percentage w/w of the xerogel on the total weight was calculated.

2.4. Attenuated total reflectance (ATR) FTIR spectroscopy

FTIR spectra of pNIPAAM hydrogel samples were collected on a FTIR spectrometer (IRAffinity-1, SHIMADZU™, Japan) using a single reflectance ATR cell (MIRacle™ 10, equipped with a diamond/ZnSe crystal). All data were recorded at room temperature, in the spectral range of 4000–700 cm^{-1}, by accumulating 45 scans with a resolution of 4 cm^{-1}. In order to obtain spectra of the wet hydrogel, a slice of material was put on the ATR plate. Moreover, a hydrogel sample was dried in air for 2 days at room temperature and subsequently at 70 °C for 30 min. The obtained xerogel was milled manually in order to obtain a raw particulate that was used to record the spectra.

2.5. Scanning electron microscopy

The surface morphology of the hydrogel was studied using a scanning electron microscope (EVO™MA10 Scanning Electron Microscope, ZEISS, Germany) with an acceleration voltage of 10 kV. Specimens of the hydrogel were prepared as follows: excess water was removed from the hydrogel by gentle air flux and samples were glued to the brass holders and coated with gold for 40 s using a coating machine (Q150R, QUORUM Technologies, Ashford, UK) prior to the SEM examination.

2.6. Refractive index

The refractive index of the hydrogel was obtained at room temperature by means of the prism method, by using light from a 632.8 nm He–Ne laser. An empty 30° prism container, made of microscope glass slides of constant thickness, was used for the measurement. The bottom and top part of the prism was filled with hydrogel material and water, respectively. The laser ray deviated by a δ_w angle (by water) and by a δ_h angle (by the hydrogel) when it passed through the water-filled region and the hydrogel-filled region of the prism, respectively. The refractive index of the hydrogel n_h is related to the water refractive index n_w and to the one of the air n_0 in terms of the δ_h and δ_w angles by the following equation:

$$n_h - n_w = 2n_0 \sin\left(\frac{\delta_h - \delta_w}{2}\right)\cos\delta\left(\frac{1}{\tan\alpha} - \tan\delta\right), \quad (1)$$

where α is the angle of the prism and $\delta = (\delta_h + \delta_w)/2$ [29]. Because of the thin water film on the surface of the pNIPAAM hydrogel sample, methods based on the Brewster's angle [30] were ineffective as they provided the refractive index of water. Nonetheless, the measurement of the refractive index n_x of the xerogel, obtained by drying a hydrogel sample at room temperature, was carried out by measuring the Brewster's angle using a polarized light from a 632.8 nm He–Ne laser. The Brewster's angle θ_B of the hydrogel was measured by minimizing the reflected light, thus resulting:

$$n_x = n_0 \tan\theta_B. \quad (2)$$

2.7. Compression testing

The compression force tests were performed by using a tabletop Instron™ equipment (Model 4464, ITW Test and Measurement Italy S.r.l.) with a load cell of 1 kN range. A cross-head speed of 1 mm/min was used for all of the specimens tested. The excess of water around the sample was removed by gentle air flux and the sample was cut using a falcon tube as mold (sample dimensions: thickness 4.3 mm and diameter 14.33 mm). The test was performed by using as anvil a block of metal and the hydrogel was put in a polystyrene Petri dish. The indentation probe was a cylindrical stainless steel block (∅39.95 mm). Data were recorded by Labview™ 8.6 software (Labview Professional Development System, National Instrument, TX, Austin) and processed by using Matlab™ (MA, Natick).

2.8. Tensile testing

The tensile force tests were performed by using the same equipment used for the compression force tests. The hydrogel was molded in cylindrical shaped specimens. As such, sufficient care had to be taken in preparing and then gripping the tensile specimens in order to avoid severe damage. In this study, we prepared the specimens in the following way. First, the excess of water around the sample was removed by a gentle air flux. Second, the sample ends were glued to scotch tape in order to improve the clamping efficiency. The resulting specimens were of standard dimensions, i.e. with length of 45 mm and diameter of 5 mm, which were measured by using a digital micrometer (with a precision of 1 mm). The tensile strains were obtained by dividing the crosshead displacements by the original length (45 mm) and the tensile stress was obtained by normalizing the tensile force with the section area (19.6 mm^2). Data were recorded and processed with the same software used previously in the compression force measurements.

2.9. Rheological characterization

Rheological measurements were performed by using an Anton Paar Physica™ MCR301 (Graz, Austria) rheometer, equipped with CTD450 temperature control unit, with parallel plate geometry (25 mm diameter). In order to avoid the hydrogel skidding during the measurement, the bottom part of the parallel plate sensor had a rough surface obtained with a coating of aluminum oxide particles (average diameter 0.2 mm). The influence of past stress and thermal history was ruled out by replacing the sample in the sensor system with an untreated one after each measurement set at the selected temperature. Frequency sweep experiments were carried out in the range of 0.01–10 Hz, in linear viscoelastic conditions [31]. To this aim, the value of the stress was varied to keep the value of the strain at 0.05%, as validated by strain amplitude sweep experiments that showed non-linear effects starting from a strain of 1%. The real G' (storage modulus) and imaginary G'' (loss modulus) components of the complex modulus G^* [32–35] were measured. Major issues in characterizing hydrogels were due to evaporation during the measurement and changes of water absorption during heating/cooling processes. Because of the quite rapid changes of the water-absorption capability of pNIPAAM hydrogel (even for small temperature variations), each sample was dipped in a water reservoir both while reaching the thermal equilibrium and during the whole measurement session, at the selected temperature. In a typical procedure a Petri dish (140 mm diameter) containing the pNIPAAM hydrogel and an excess of water was housed in an aluminum custom sample-holder (Fig. 1a). Such sample-holder was hermetically sealed and immersed in the thermostatic bath, for a selected time at temperature

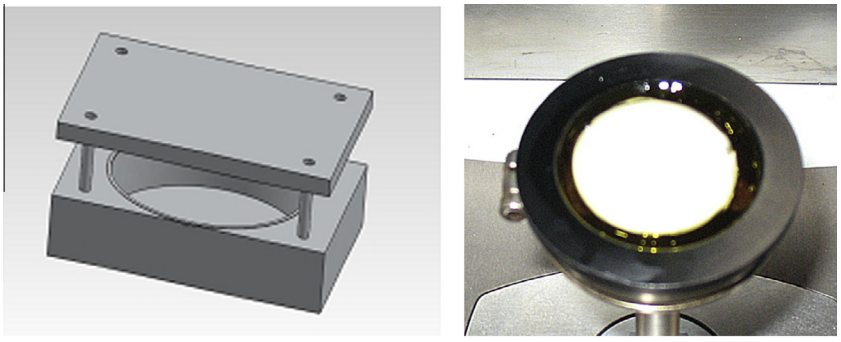

Fig. 1. (a) 3D exploded view of the aluminum hermetic sample-holder used to immerse the hydrogel in the thermostatic bath: a Petri dish (∅140 mm) containing the hydrogel material was housed at the centre of the container before hermetic closing and (b) pNIPAAM sample covered by an oil layer and placed on the rheometer bottom sensor at the end of a measurement session.

T. Then the sample was cut and transferred for the measurement into the rheometer, preset at the same temperature *T*. The bottom part of the measuring system was a cup filled with water where the sample and top sensor were plunged. Finally, a thin layer of oil was created on the water surface to prevent evaporation from the measuring system [36] (Fig. 1b). Preliminary tests at room temperature showed that the presence of water did not alter the measurement of G' and G'' of the hydrogel. Temperature scans of G' were also obtained at a selected frequency, varying the temperature within the rheometer at preset cooling/heating rates. This experimental setup allowed us to be confident about the fact that during the measurements the hydrogel was fully hydrated.

3. Theory

The mechanical properties of a lightly crosslinked hydrogel can be described starting from the thermodynamic treatment of rubber elasticity. In their swollen form, hydrogels respond to stress with nearly instantaneous and fully reversible (if they are not too high) deformation because of rapid rearrangements of polymer strands. General characteristics of rubber elastic behavior include high extensibility, caused by low mechanical stress, and complete recovery after removal of external loads. High extensibility and recovery are driven by entropic rather than enthalpic changes [37].

Rubber elasticity may be described in a classic thermodynamic framework [38] by the state Eq. (3) at the temperature *T*

$$f = \left.\frac{\partial U}{\partial L}\right|_{V,T} - T\left.\frac{\partial S}{\partial L}\right|_{V,T}, \tag{3}$$

where *f* is the force exerted by the elastomer to maintain a certain configuration, when it has a length *L*, a cross-section *A*, and a volume $V = AL$. In the case of ideal rubber elastic behavior, it can be safely assumed an invariant internal energy [39]: in fact, it can be assumed that the chain bonds are not stretched with changes of *L*.

Entropy for a single chain can be obtained as $s = k_B \ln Z(x,y,z)$, where $Z(x, y, z)$ is the partition function representing the number of conformations available for the chain if the end-to-end vector is (x, y, z). For a mobile chain the probability distribution in space of the end-to-end vector is given by a Gaussian [40] described by the following equation:

$$p(x,y,z) \sim Z(x,y,z) \sim \exp\left(-\frac{3(x^2+y^2+z^2)}{2R_0^2}\right), \tag{4}$$

where R_0^2 is the mean-squared end-to-end distance of the chain.

A generalization to an ensemble of polymer chains of bulk density ρ can be done with the following assumptions:

1. all the chains in the network have the same degree of polymerization and carry crosslinks only at their ends (this means that the mass between crosslinks is a constant, namely M_c);
2. the conformational distribution in the undeformed state agrees with that of an uncrosslinked melt (i.e. Gaussian distribution);
3. fixed crosslinks that change their position in an affine way with the sample deformation.

In this framework, let us consider the orthogonal deformation of the sample $(x,y,z) \to (\lambda_x x, \lambda_y y, \lambda_z z)$. In the case of uniaxial extension in *z*-direction with $\lambda_z = \lambda$, considering the sample as incompressible and isotropic, one has $\lambda_x = \lambda_y = 1/\sqrt{\lambda}$. Under these conditions, the entropy of a deformed sample results

$$\begin{aligned} S &= Vc \int s(x,y,z)p\left(\frac{x}{\sqrt{\lambda}}, \frac{y}{\sqrt{\lambda}}, \lambda z\right) \mathrm{d}x\,\mathrm{d}y\mathrm{d}z \\ &= -Vc\frac{k_B}{2}\left(\frac{2}{\lambda} + \lambda^2 - 3\right), \end{aligned} \tag{5}$$

where *c* is the concentration of strands/chains.

Therefore, the Young modulus *E* in the linear response regime can be calculated in terms of the stress σ and the strain ε as

$$\sigma = \frac{f}{A/\lambda} = -\frac{\lambda T}{A}\left.\frac{\partial S}{\partial L}\right|_{V,T} = -\frac{\lambda T}{AL}\left.\frac{\partial S}{\partial \lambda}\right|_{V,T} = ck_BT\left(\lambda^2 - \frac{1}{\lambda}\right), \tag{6}$$

$$\varepsilon = \frac{\lambda L - L}{L} = \lambda - 1, \tag{7}$$

$$E = \lim_{\varepsilon\to 0}\frac{\sigma}{\varepsilon} = \lim_{\lambda\to 1} ck_BT\frac{\lambda^3 - 1}{\lambda}\frac{1}{\lambda - 1} = 3ck_BT = 3\frac{\rho RT}{M_c}. \tag{8}$$

Having assumed incompressibility (Poisson's ratio of 0.5) [41], the shear modulus is

$$G = \frac{1}{3}E = \frac{\rho RT}{M_c}. \tag{9}$$

Several models were developed in the literature to improve Eq. (9) to be applicable in less restrictive experimental cases [42,43]. These deviations can be taken into account in invariant-based continuum mechanics treatments such as the Mooney–Rivlin model [44,45] that provides for the nominal stress $\hat{\sigma}$ (also called engineering stress)

$$\hat{\sigma} = \frac{f}{A} = \frac{\sigma}{\lambda} = 2\left(\lambda - \frac{1}{\lambda^2}\right)\left(C_1 + \frac{C_2}{\lambda}\right), \tag{10}$$

where C_1 and C_2 are material constants often referred to as Mooney–Rivlin coefficients. It is worth noting that if $C_2 = 0$ in Eq.

(10), the same functional dependence of Eq. (6) is recovered. This condition provides the nominal stress $\hat{\sigma}$ for the neo-Hookian model, in which $2C_1$ is the shear modulus G:

$$\hat{\sigma} = G\left(\lambda - \frac{1}{\lambda^2}\right). \tag{11}$$

Determination of C_1 and C_2 of Eq. (10) in terms of material parameters becomes more and more complex when the ideal assumptions above are progressively removed [28] or other features are taken into account.

Among others, we recall the Flory treatment for defects of the network introducing in the expressions of moduli in Eqs. (8) and (9) a factor $1 - 2M_c/M_n$ [46]. Entanglements are considered in the models of Langley [47], Dossin and Graessley [48–50]. Deviations from the Gaussian behavior due to interactions or constraints of neighboring chains occurring at increasing deformations are taken into account in the Flory–Erman treatment of constrained junction fluctuation model [51]. Moreover, solutions of polymers can be considered [52] leading to the Frenkel–Flory–Rehner theory [53,54] for the swelling of polymer networks.

As a final result, if the effects of entanglements are neglected, the shear modulus can be written as [28,37]

$$G = Q\frac{N_e}{V_x}RT\left(\frac{V_x}{V}\right)^{\frac{1}{3}}, \tag{12}$$

where Q is a dimensionless constant roughly independent of the temperature and only dependent on solvent-polymer network characteristic (such as the crosslink functionalization f, or the molar volume of the solvent); V and V_x are the undeformed volumes of swollen and "dry" polymer network (i.e. xerogel), respectively; N_e/V_x is the concentration of elastically active chains (for a perfect network, the number of crosslinks is $2N_e/f$ [28]).

4. Results and discussion

4.1. Water absorption

Xerogel uptake of water was studied after 2 days of equilibration. Results showed that the xerogel/hydrogel weight ratio was of (4.5 ± 0.1)%. Moreover, the xerogel volume fraction ϕ_x was found to be (3.7 ± 0.1)%.

4.2. Attenuated total reflectance (ATR) FTIR spectroscopy

The hydrogel FTIR spectrum (see the electronic Supplementary material) showed a broad band for H-bond around 3300 cm^{-1} due to the hydrogen bond network between trapped water and amide groups in polymer chain. Typical C=O stretching vibration in amide groups were well visible around 1627 cm^{-1} together with the N—H bending at 1558 cm^{-1}. In the fingerprint region the strongest signal was for C—N stretching, around 1462 cm^{-1}. The xerogel FTIR spectrum was more complicated: at around 3282 cm^{-1} we observed the peak of N—H stretching, while around 2930 cm^{-1} it was possible to notice the CH region. We were able to recognize also in the xerogel the C=O stretching and the N—H bending exactly in the same position of the hydrogel. Moreover, close to the more intense C—N stretching around 1458 cm^{-1}, it was possible to identify: at around 1380 cm^{-1}, the CH_3 umbrella deformation and, at 1130 cm^{-1}, the CH_3 rocking.

4.3. Scanning electron microscopy imaging

Fig. 2 shows the SEM photos of the surface structure of the gel samples. Conversely to the already published results reported by Suzuki et al. in 1996 [55] we decided to not freeze-dry the hydrogel before performing SEM analysis, in order to avoid structure destruction due to the sublimation of water from the polymer network. To the best of our knowledge this is the first time pNIPAAM hydrogel is observed using SEM without prior freeze drying [55] as a main results it is possible to see intact network structures, without any dramatic freezing effect. In this way, we obtained images with about 10 μm pore size with good resolution with a regular distribution of pores in the material (pore size gradients visible in the SEM images are due mainly to the positioning of the sample on the sample carrier).

4.4. Refractive index

The results obtained by means of the prism method consisted in $n_h - n_w = 0.005 \pm 0.001$ for the pNIPAAM hydrogel. As regards the xerogel sample at room temperature we found a Brewster's angle $\theta_B = 56°40' \pm 30'$ (see electronic Supplementary material). Therefore, $n_x = 1.520 \pm 0.035$, corresponding to the value given for pNIPAM xerogel bulk after extrapolation of literature data [56–58]. According to the Maxwell–Garnett mixing rule [59,60] the refractive index of the hydrogel can be written in terms of the refractive indexes of the water and the gel as [56]

$$n_h = \phi_w n_w + \phi_x n_x, \tag{13}$$

where $\phi_w = 1 - \phi_x$ and ϕ_x are the bound water volume fraction and the xerogel volume fraction, respectively. Substituting the measured value of $n_h - n_w$ and considering $n_x = 1.52$ in Eq. (13), we obtained:

$$\phi_x = \frac{n_h - n_w}{n_x - n_w} = \frac{0.005 \pm 0.001}{0.19 \pm 0.04} = (2.6 \pm 0.7)\%. \tag{14}$$

This value for the xerogel volume fraction is compatible with that obtained from water absorption studies, i.e. (3.7 ± 0.1)% (see Section 4.1).

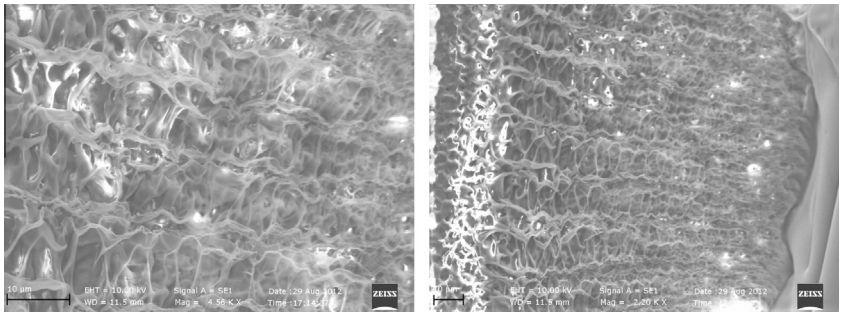

Fig. 2. SEM micrographs of pNIPAAM hydrogels. The scale bar is 10 μm.

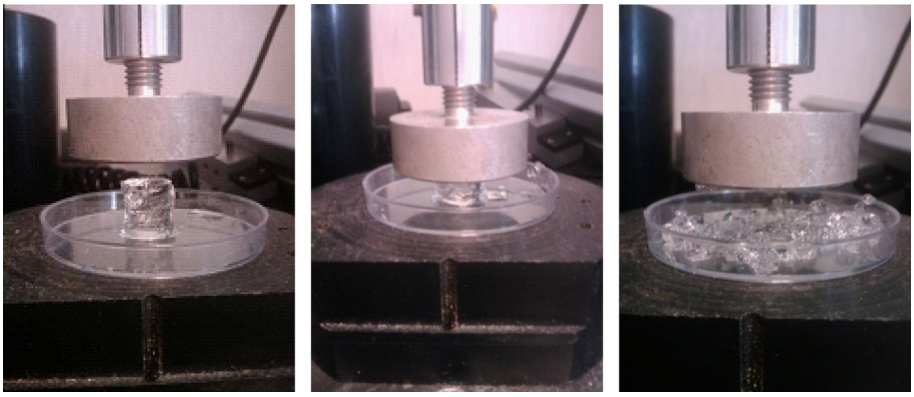

Fig. 3. From left to right, photograph sequence illustrating the behavior of a hydrogel cylindrical sample when subjected to a compressive uniaxial force by means of a cylindrical stainless steel indentation probe: (left) starting phase, (middle) during compression and (right) after specimen failure.

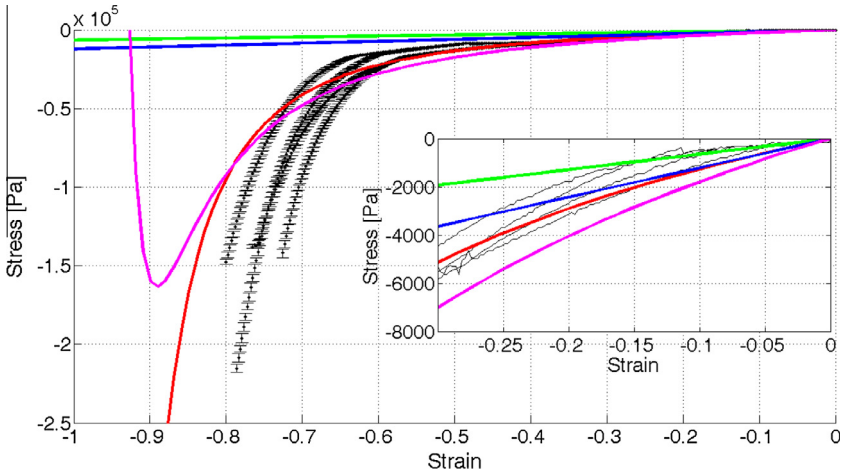

Fig. 4. Graph showing the results of the compression tests where data is shown with error bars for four typical samples. The different types of fitting curves are indicated: linear hookean at 15% strain (green); neo-hookean (red); Mooney–Rivlin (magenta). Inset: detail showing strains between 0% and 30%. Data are related to engineering type of stress and strain. Error bars of the data have been removed and data points for same samples were connected to improve visual clarity. (For interpretation of the references to color in this figure legend, the reader is referred to the web version of this article.)

4.5. Compression tests

The typical sequence of compression experiments for the gel is reported in Fig. 3. The material deforms in response to the application of the compression force until the break point, at a maximum compression force. In Fig. 4, we report the typical results of four tests and three models are proposed to describe the mechanical properties. The behavior of hydrogel can be divided in three regions: hookean relation is in good agreement with the stress/strain curve until 30% of deformation. The elastic modulus E_c was calculated, with linear regression, up to 15% and up to 30% of material deformation, corresponding to 6.5 kPa and 12.2 kPa, respectively. The neo-Hookean G_c is calculated to be 3.8 kPa, with little difference from the one reported by Gundogan et al. [17]. This difference is probably due to the fact that in [17] the polymerization reaction was performed at 5 °C, while in our work we used 25 °C as reported in the experimental part. At low temperature polymerization kinetics is slower, so the material is formed by a lower number of polymer chains and the G_c modulus is higher. From our extrapolations, we obtain a ratio $E_c^{30\%}/G_c = 3.2 \pm 0.3$ that is very close to the theoretical ratio of 3 for incompressible materials. Mooney–Rivlin equation is giving comparable results to the neo-Hookean treatment. The material is able to resist to compressive stresses till the 79% of the total strain.

4.6. Tension tests

Tensile tests were performed in this work for the first time on the pure pNIPAAM hydrogel. Results are shown in Fig. 5. Tensile experiments gave less accurate data than compression tests but it was still possible to estimate both the Young modulus, E_t, and the neo-hookean modulus, G_t, as 24.8 kPa for 15% of elongation and 7.3 kPa, respectively. In this case the ratio $E_t^{15\%}/G_t = 3.4 \pm 0.1$ which confirms the incompressibility assumption made in the derivation of the Neo-Hookean model. These values are quite in agreement with the results available in literature, which, to our knowledge, can only be found in [19] in presence of latex particles. Moreover, from our experimental analysis it was not possible to estimate the value of E_t for 30% of elongation because the breaking point of some hydrogel samples falls within the 30% elongation range. Furthermore Mooney–Rivlin model does not seem to be adequate to fit these data, according to the low rupture limit of the material.

Differences of behavior between compression and tensile experiments are probably due to the dramatically different water behavior in hydrogel matrices when the two different types of mechanical stimulation are provided. It can be interpreted that while when applying an external compressive force the water is re-distributed in the hydrogel matrix, somewhat improving the

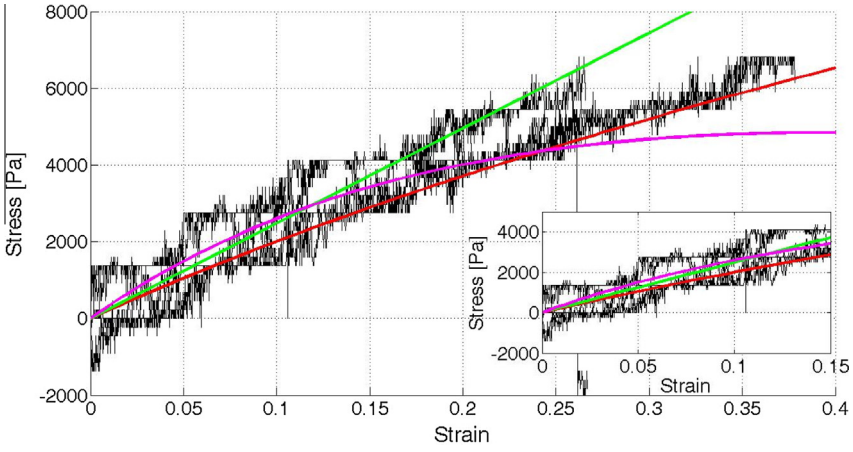

Fig. 5. Graph showing the results of the tension tests where data is shown for five typical samples. Typical measurement accuracy was ±0.35 kPa The different types of fitting curves are indicated: linear hookean at 15% strain (green); neo-hookean (red); Mooney–Rivlin (magenta). Inset: detail showing strains between 0% and 15%. (For interpretation of the references to color in this figure legend, the reader is referred to the web version of this article.)

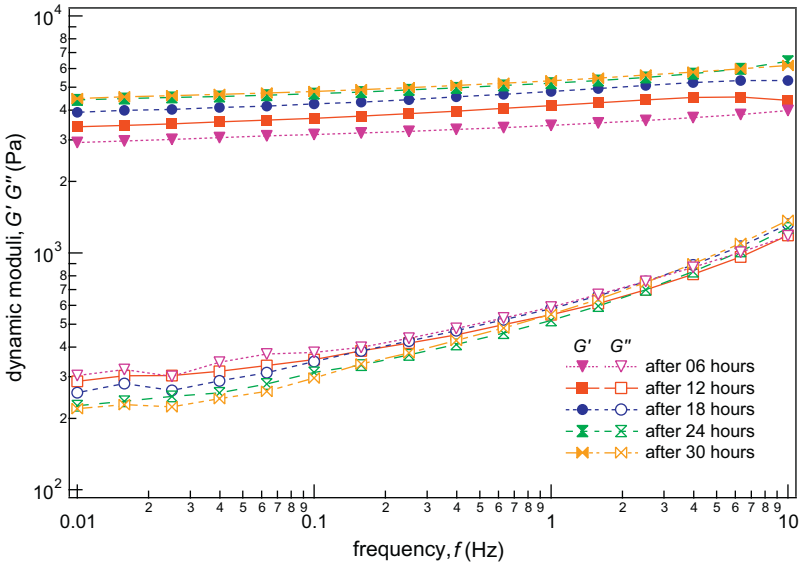

Fig. 6. Evolution with time of the storage and loss moduli of pNIPAAM measured at the constant temperature of 36 °C. The dynamic moduli reach a stationary state after 24 h.

elastic behavior of the material, the water redistribution probably does not affect in such a great extent the elastic behavior in tensile experiments, thus the specimens had an earlier rupture point. In particular, from those experiments in which material failure was investigated it could be observed that the specimens start to lose their external skin characteristics in several parts, thus contributing to the more rigid behavior. This also affects the measurements by introducing noise, clearly evident in Fig. 5. A further source for the large noise observed is due to the imperfect clamping, unavoidable because of the nature of the material under investigation. In addition it was not possible to get any hysteresis measurement because the tensile experiment, even for little deformations, already produced visible shredding on the material, compromising the possibility to perform cyclic testing.

4.7. Rheological tests and their microscopic interpretation

Preliminary dynamic rheological studies on pNIPAAM macrohydrogel were focused on studying the time evolution of G' and G'' in frequency sweep measurements at the swelling–deswelling transition. Fig. 6 shows the time evolution of the dynamic shear moduli of the gel for frequency sweep measurements carried out at the constant temperature of 36 °C. After 24 h G' and G'' were stable, so that we were confident in carrying out all the experiments for temperatures higher than 30 °C, after maintaining the samples at the selected temperature for 30 h. The choice was also supported by the consideration that the temperature of 30.6 °C corresponds to the Θ Flory temperature for pNIPAAM in water [52,61]. The trend observed in Fig. 6 shows that the elastic response of the hydrogel increases with time, while the material reaches thermal stability by finishing its phase transition.

In Fig. 7, we show the time behavior towards the equilibrium of $G'(0.1\ \text{Hz})$ for different temperatures. The modulus reached the equilibrium according to an exponential law with characteristic times τ of the order of hundreds of minutes. In particular, the finding for 44 °C was in nice agreement with literature results [62].

We compare frequency sweep curves for the gel at temperatures above and below its transition in Fig. 8. The reproducibility of the measurements was carefully verified. The shrinking of the chains above the transition resulted in the increase of one order of magnitude of the value of both storage and loss modulus. As a first result, it is apparent the almost full elastic response of

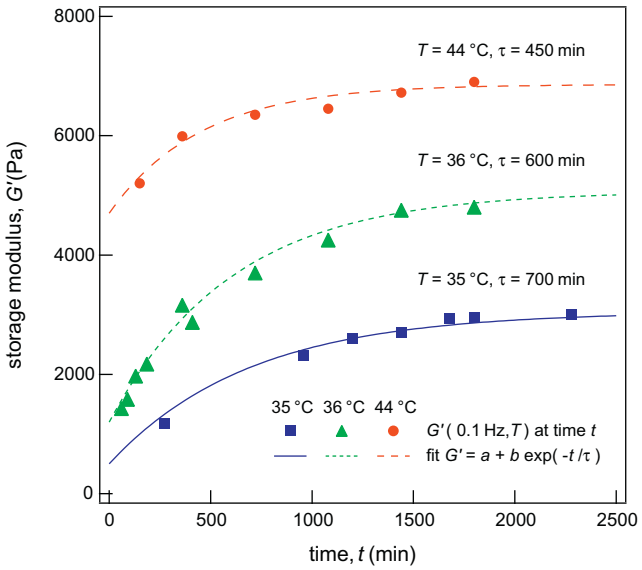

Fig. 7. Time evolution of the storage modulus at 0.1 Hz resulting from experiments performed at different temperatures.

pNIPAAM resulting in a storage modulus strongly greater than loss modulus: in particular, at 0.1 Hz, G'' is one order of magnitude smaller than G'. Moreover, it was possible to notice the thermorheological complexity of the hydrogel response: in fact, any attempt to reconstruct a master curve applying the time temperature superposition principle [39] failed, even for separate regions of temperature below and above transition.

The swelling–deswelling transition can be appreciated looking at the temperature behavior of the storage modulus of pNIPAAM hydrogel. Fig. 9 reports G' measurements under different experimental conditions: in all cases a transition from soft to harder values of the modulus was observed as the temperature increases through the transition.

In Fig. 9 the full squares refer to G' at 0.1 Hz from the frequency sweep experiments carried out in the thermally stationary state and after maintaining the sample at the selected temperature for 30 h. Similar curves can be produced at different frequencies, showing the same shape and amount of information due to lack of a structure in the frequency sweep curves. From the maximum of the slope of these G' data versus temperature, we determined

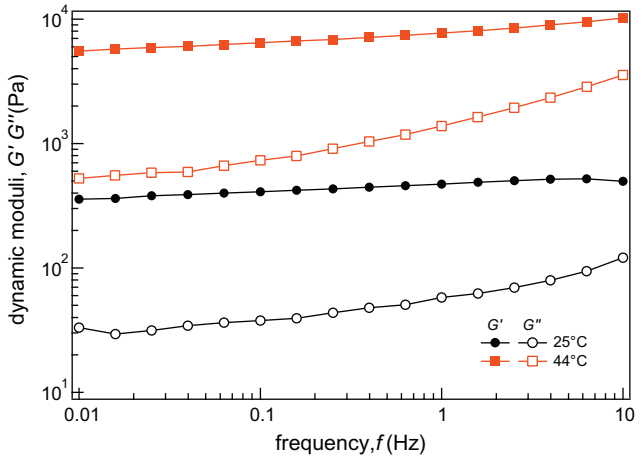

Fig. 8. Frequency sweep curves of shear moduli G' and G'' at temperatures above and below the swelling–deswelling transition.

the transition temperature T_{infl} = 35 °C (Fig. 10). It is worth noting that the G' derivative curve exhibited at 30.1 °C a plateau towards low temperatures, in nice correspondence with the Θ Flory temperature of pNIPAAM in water.

Coming back to other experimental protocols applied in this work, temperature sweep experiments were performed to study the storage modulus of pNIPAAM samples both while cooling it from above the transition temperature and heating it from below, in both cases varying temperatures by 1 °C every 12 h. The results are shown in Fig. 9 as the long-dashed line in orange (color online) and the dashed-dotted line in green (color online) respectively, and were well matched by the data points obtained in the thermally-equilibrated frequency sweeps, evidencing that the slow rate of the experiment allowed the sample to reach the thermal equilibrium step by step. In the case of the heating experiment, we observed an artefact in the G' value after Θ temperature, which is caused by the progressive shrinking of the sample as it approached the transition temperature.

In Fig. 9 we also show data from a temperature loop experiment for G' at 0.1 Hz, performed by initially cooling the sample from 45 °C to 30 °C and then heating it up to 45 °C at 6 °C/h. A hysteresis is observed, that could be explained as follows. On cooling, the rate of the temperature perturbation was greater than the rate of the microscopic rearrangement of the gel structure, so that G' always remains above its equilibrium values and reaches an out-of-equilibrium plateau value below the transition, due to incomplete swelling of the hydrogel. This was in agreement with the relaxation times for equilibration: in fact the time for the cooling temperature ramp was 150 min, while we found at 44 °C τ = 450 min, implying that not even staying at the highest temperature for this period of time the equilibrium would have been reached. On the other hand, on re-heating, the deswelling process proceeded starting from a partly deswelled state of the material, being therefore able to recover its equilibrium values during the heating, even if the same absolute value of the cooling rate was applied in the temperature sweep.

The measurements of the G' temperature dependence at 0.1 Hz were also compared to the hydrogel volume changes with temperature. To this regard, volumes were estimated after measuring the dimensions of the samples: the diameters of the pNIPAAM cylinders were evaluated before placing the samples in the rheometer sensors and after the cutting procedure, which was carried out with a mold of 25 mm diameter, while the cylinder heights were more precisely measured by the rheometer itself. The error over the volumes can be confidently set as 15%.

Data are presented in Fig. 11, where we rescaled the storage modulus as the dimensionless quantity $G'(T)/G'(T_0)$ and the volume as the ratio $V(T_0)/V(T)$, as a function of temperature, with T_0 = 25 °C. Despite the rough estimation of pNIPAAM hydrogel volume, satisfactory agreement was observed between rescaled G' and the rescaled ratio $V(T_0)/V(T)$. This result is in agreement with both the scaling theory [63] in good solvents and the Flory–Huggins theory [52]. In fact, from Eq. (12) it is found

$$\frac{G'(T)}{G'(T_0)} = \frac{N_e(T)}{N_e(T_0)} \frac{T}{T_0} \left(\frac{V(T_0)}{V(T)} \right)^{1/3}, \tag{15}$$

where the temperature ratio is calculated using the absolute temperature scale, and N_e is the number of elastically active chains. It is known that this number scales as $\phi_x^{5/3}$ in good solvent conditions [52]. Therefore, in the present case it is found

$$\frac{G'(T)}{T} \frac{T_0}{G'(T_0)} = \left(\frac{V(T_0)}{V(T)} \right)^n \tag{16}$$

where n is expected to be 2.

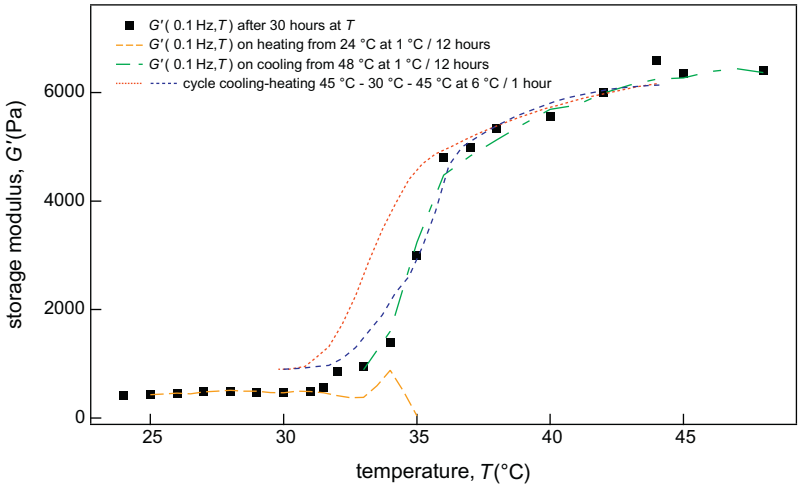

Fig. 9. Temperature dependence of the storage modulus of pNIPAAM at 0.1 Hz according to different thermal treatments.

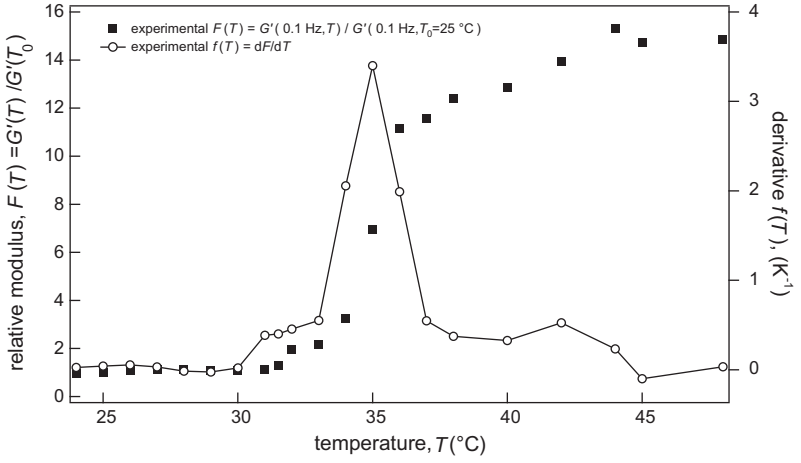

Fig. 10. Temperature dependence of the rescaled storage modulus of pNIPAAM at the stationary state (full square) and its derivative for evaluation of the transition temperature.

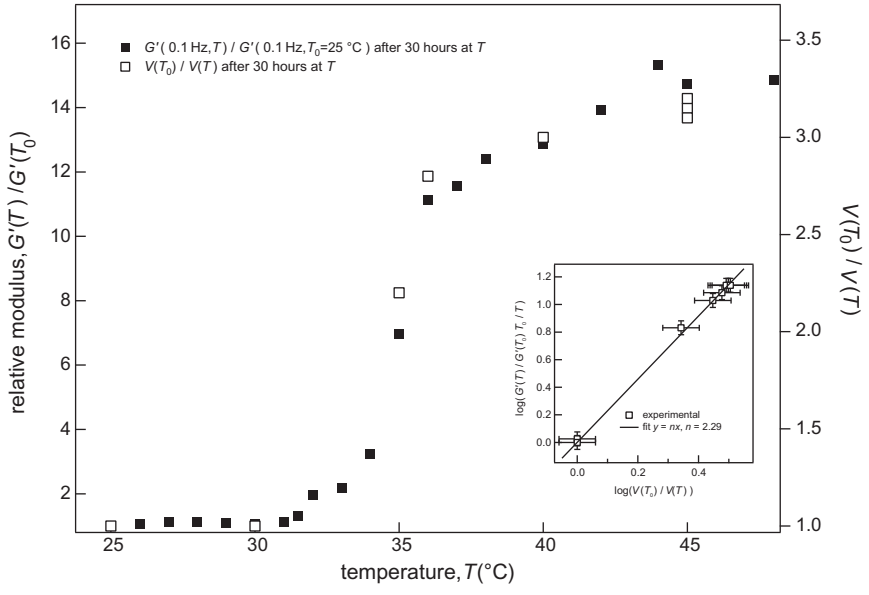

Fig. 11. Comparison of temperature dependence of rescaled storage modulus G' and rescaled inverse volume of the pNIPAAM through the swelling–deswelling transition. In the inset the bilogarithmic plot supports the presence of a scaling law with exponent $n \approx 2$ according to Eq. (16).

The presence of a scaling law can be appreciated in the inset of Fig. 11, where experimental data for $(G'(T)/G'(T_0))/(T_0/T)$ were plotted versus $V(T_0)/V(T)$ in a bilogarithmic graph. A linear fit provided the exponent $n = 2.29$ in good agreement with literature results on gels [28].

To get more insight on the swelling–deswelling transition around 35 °C, according to Eq. (16) the temperature dependence of the polymer volume fraction $\phi_x(T)$ was obtained from the experimental storage modulus $G'(T)$ as

$$\phi_x(T) = \phi_x(T_0)\left(\frac{G'(T)}{T}\frac{T_0}{G'(T_0)}\right)^{1/n} \tag{17}$$

The temperature dependence of $\phi_x(T)$ is shown in Fig. 12. Polymer volume fraction data were thus compared with different models from the literature: a phenomenological model for sigmoid-shaped transitions and some theoretical models, namely approximated single chain, single chain, affine network, perfect affine network, phantom network and constrained junction fluctuation (CJF) models.

Initially, we took in consideration a phenomenological description for sigmoid-shaped transitions, often employed in theories for thermodynamic second-order transitions such as the glass transition [64,65]. In this model $\phi_x(T)$ can be written as [66]:

$$\phi_x(T) = M + \frac{m - M}{1 + e^{\frac{T - T_{infl}}{D}}}, \tag{18}$$

where T_{infl} is the inflection or transition temperature, D is a parameter related to the width of the transition, and M and m are the maximum (horizontal asymptot at high temperature) and the minimum (plateau at low temperature) of the curve, respectively. The fit with this phenomenological model (dashed-dotted orange line in Fig. 12, color online) signals a sharp transition with $D = 1.1$ °C at the temperature $T_{infl} = 34.6$ °C, in agreement with T_{infl} inferred from Fig. 10. The reduced chi-square, χ^2_r, of the fit was 0.6.

Models based on statistical theories have been proposed in the literature starting from Flory theories [28,52]. These models originated from the equation

$$\ln(1 - \phi_x) + \phi_x + \chi\phi_x^2 + C\phi_x^{1/3} = 0 \tag{19}$$

where χ is a parameter that linearly depends on the temperature, and C a parameter that can depend on ϕ_x and also on polymer architecture, polymer–solvent characteristics, and swelling conditions.

One of the simplest models derived from Eq. (19) is an approximation used for a single chain in solution [67]. Such a model had a single fit parameter, namely the ratio M_w/M_0, where M_0 is the molar mass of residues, which may be one monomer unit or a number of repeating units grouped together [67]. In the case of the hydrogel studied in this work, we found $M_w/M_0 = 34{,}000$ and a reduced chi-square of 3.5, signaling a poor fit. In fact, the corresponding curve (long-dashed green line in Fig. 12, color online) approximates the experimental data only at temperatures near the Flory temperature, confirming that assumptions of diluted solution and single-chain result totally inadequate for the pNIPAAM hydrogel.

By removing the assumption of diluted solution we can work with the single chain model, maintaining both a linear dependence on temperature for χ and affine deformation, as assumed in the approximated model for the single chain. Consequently, the explicit functional form of χ and C in Eq. (19) becomes [28]: $\chi = A + BT$ and $C = K(1 - \phi_x^{2/3})$, where the parameter K only depends on polymer-solution material quantities. By inspection of Fig. 12, this model improved substantially the quality of the fit (short-dashed purple line, color online) through the whole transition zone, but the behavior still maintained an increasing trend at higher temperatures, providing a reduced chi-square of 3.0. The fact that, with the single chains models, the high-temperature plateau cannot be recovered suggests that the network nature of the hydrogel has to be taken into account in a different way.

To improve applicability of Eq. (19) for hydrogels, a revision of the χ parameter [68] has shown to be effective for pNIPAAM networks [69,70]. Accordingly

$$\chi = \chi_1 + \chi_2\phi_x = A_1 + B_1T + A_2\phi_x + B_2T\phi_x \tag{20}$$

We tested this behavior in the case of two limit models describing polymer networks: the affine model [28,71] and the phantom model [28,71,72]. The phantom model foresees $C = K$ in Eq. (19), while the affine model provides

$$C = K\left(1 - \frac{N_c}{\xi}\phi_x^{2/3}\right) \tag{21}$$

in Eq. (19), where N_c is the number of crosslinks and ξ the number of independent circuits in the network.

In addition, the CJF model [73–75] can be considered, which tries to reproduce real networks and, in the case of free-swelling, sets

$$C = K(1 + g(\zeta, \kappa, \phi_x)) \tag{22}$$

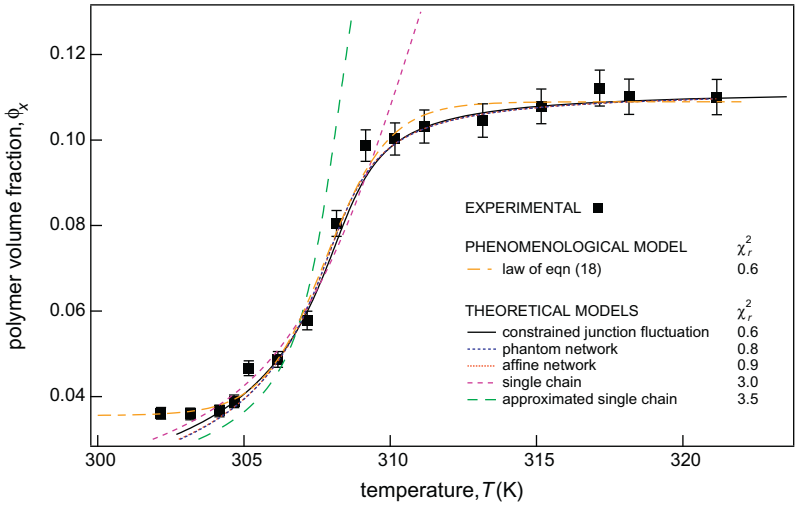

Fig. 12. Comparison of the experimental polymer volume fractions and theoretical models for the gel.

where g is a function whose expression was detailed elsewhere [28], ζ is a parameter characterizing the non-affine behavior, and κ is a parameter expressing the "strength" of the interaction with surrounding chains. At the two limiting values for the κ range, namely 0 and ∞, CJF model recovers phantom and affine models, respectively.

In all the cases, K can be written as $K = \xi v_{H_2O}/(N_A V_x(T_0))$, where N_A is the Avogadro's number, and v_{H_2O} is the molar volume of the solvent.

In the presence of a "perfect" network [28], ξ can be written as $\xi = N_e - N_c + 1$ and it is also possible to set $N_e = N_c f/2$, where f is the number of chains emanating from a network junction. After assuming $f = 4$, $\xi = N_c + 1$, therefore N_c/ξ is found to tend to 1 for perfect networks and $\xi \cong N_e/2$. Moreover, starting from a rough definition of the average molar mass between crosslinks given in the literature as $M_c \cong \rho N_A V_x(T_0)/N_e$ [28], it can be set for perfect networks:

$$\frac{\rho v_{H_2O}}{2M_c} \sim K \tag{23}$$

In this work, we also studied the perfect network case of the affine model.

Best-fit curves and parameters for all these models are reported in Fig. 12 and in Table 1, respectively. As a very remarkable result it is possible to see that the introduction of the ϕ_x-dependent term in χ according to Eq. (20) allows Eq. (19) to recover the high temperature plateau. Fitting procedures according to the affine network model treated N_c/ξ as a free parameter, and provided the value 0.91, very near the ideal $N_c/\xi = 1$ case (Table 1). On the other hand, the perfect affine network model was handled after constraining $N_c/\xi = 1$ in the affine model.

The affine network, the perfect affine network and the phantom network models provide almost identical best-fit curves. Nonetheless, because of the number of fit parameters, the reduced chi-square of the phantom network model turns out to be less than the one found for the affine network model. Note that the reduced chi-square of the perfect affine network and the phantom models are coincident because of the matching in the number of fit parameters. However, no significant change in the quality of the fit was obtained because we did not introduce at the same time constraints about K.

The data in Table 1 evidence that the best fit was obtained, as one could have expected, by the CJF model, which provided a mixing of the two limiting affine and phantom cases. It is also worth noting that this last statistical model provided a reduced chi-square of 0.6, the same as the phenomenological curve discussed previously.

Inspection of the parameters given in Table 1 allows us to conclude that that addition of the ϕ_x-dependent term in Eq. (20) is determinant in obtaining good-quality fits. Interestingly enough, the A_i and B_i parameters, $i = \{1, 2\}$, of Eq. (20) are quite independent of the network model employed in the fitting procedure. This confirms the "thermodynamic" nature of the χ parameter, not influenced by the character of the polymer network. Moreover, the signs of the A_i and B_i parameters gave the same indication and were the same as the ones found in literature [69] for a similar hydrogel.

Even if CJF model provides the best fit, also the perfect affine network and affine network give very similar K values, suggesting that the affine descriptions of the network should be confidently preferred in face of the phantom network description.

With the assumption that the affine network model can be considered a good description for our hydrogel, we were able to calculate some microscopic properties of the materials. In fact, according to our findings (Table 1) and Eq. (23), it is possible to estimate a M_c value of the order of 10 kg mol^{-1}. Moreover, it is possible to evaluate the molar concentration of crosslinks remembering that in the affine network multiplication of K and N_c/ξ turns out to be $v_{H_2O}N_c/(N_A V_x)$ and thus $KN_c/\xi v_{H_2O} = 110$ mol m^{-3}.

These results are nicely able to confirm the reaction stoichiometry. In fact, starting from the stoichiometry of the synthesis and approximating reasonably the mass of the whole polymer to the total initial mass of NIPAAM monomer, we obtained as the average molar mass per crosslinker molecule the value 10.3 kg mol^{-1}, in perfect agreement with the result of our analysis about M_c.

Moreover, as far as the molar concentration of crosslinks is concerned, the evaluation of 96 mol m^{-3} was obtained, after approximating stoichiometrically the whole volume of the polymer with the volume of the total initial mass of NIPAA monomers.

The application of statistical models gave us possibility in inspection on the architectures present in pNIPAAM hydrogel treated in this work. Considering the Gaussian approximation [40], we can estimate the mesh size Δ of the swollen polymer network:

$$\Delta = l_0\left(\frac{2C_\infty M_c}{M_0}\right)^{1/2} \tag{24}$$

where l_0 is the length of the bond along the backbone chain, and C_∞ and M_0 are the Flory characteristic ratio and the molecular weight of the repeating units, respectively. In the case of pNIPAAM, we can state $M_0 = 113.6$ g mol^{-1}, $l_0 = 0.15$ nm, $C_\infty = 10.6$ [76], resulting in a mesh size of the hydrogel $\Delta = 6.5$ nm.

Taking into account a contraction $\phi_x^{1/3}$, we can also determine the mesh size Δ_x of the polymer network of the xerogel as $\Delta_x = \Delta\phi_x^{1/3} = 2.2$ nm. In turn, such a value allows us to evaluate the molar concentration of the crosslinks in the polymer melt, which is given by $1/(\Delta_x^3 N_A) = 150$ mol m^{-3} and is in nice agreement with the result obtained above from fit parameters of the affine model and from the synthesis stoichiometry.

Table 1
Best fit parameters for the statistical models of Eqs. (19)–(21).

Model	χ_r^2	$K \times 10^{-3}$	A_1	B_1 (K^{-1})	A_2	B_2 (K^{-1})	N_c/ξ	κ	ζ
Perfect affine	0.8	2.18	−84.7	0.275	758	−2.45	1.00[a]	–	–
Affine	0.9	2.22	−82.2	0.267	736	−2.38	0.91	–	–
Phantom	0.8	4.02	−81.2	0.264	727	−2.35	0.00[a]	–	–
CJF	0.6	2.53	−83.1	0.270	745	−2.41	–	2.24	1.7

[a] Constrained.

5. Conclusions

N-isopropylacrylamide (pNIPAAM) hydrogels motivate research focus because of their remarkable thermo-responsive properties which open a wide variety of applications ranging from tissue engineering and drug delivery to innovative actuation and sensing components. Therefore the understanding of the mechanical properties of this kind of hydrogel, with special attention to the viscoelastic dynamic behavior and elastic behavior, is required. Our work tried to complete the main aspects of mechanical and rheological characterization of the most common reticulated pNIPAAM hydrogel, with special attention to the integration of this information in a consistent network. In particular, main results can be summarized as follows.

The deformation response under uniaxial compression of this material was studied in water equilibrium condition up to the rupture limit. Experimental data of engineering stress–strain curves were described using hookean, neo-hookean and Mooney–Rivlin phenomenological approaches. From these studies it resulted that:

(a) the pNIPAAM hydrogel hookean response region, in presence of 1.2 mol% of crosslinker, is limited to the 30% of total deformation and it is described by a E_c modulus of 12.2 kPa;
(b) between 30% and 79% of total deformation, neo-hookean fitting is giving a G_c modulus of 3.8 kPa in good correlation with previous results [15];
(c) the Mooney–Rivlin phenomenological approach gave results comparable with the neo-hookean behavior.

From these results it is possible to confirm that neo-hookean is the most promising fitting for the phenomenological description of compressive response of pNIPAAM hydrogel.

The tensile response of pNIPAAM hydrogel was measured for the first time on the pure material, avoiding indirect calculation that suffers from the presence of the latex in the specimen used for the measurement. As a first result, hydrogel with 1.2 mol% of crosslinker was confirmed to be fragile under tensile stress, with a rupture limit around 30%. Under this limit it was possible to fit experimental data with hookean, neo-hookean and Mooney–Rivlin phenomenological approach. In this case the hookean region was limited from 0% to 15% of total deformation and is described by a E_t modulus of 24.8 kPa, while neo-hookean is giving a G_t modulus of 7.3 kPa and Mooney–Rivlin fitting is considered inappropriate due to the low rupture limit of the material. Conversely to what was observed in compressive test, hookean and neo-hookean models are equally good in describing the mechanical response, because the hyperelastic region was hidden by the early rupture.

It was not possible to fully compare uniaxial compressive and tensile results because of the pNIPAAM different rupture limits in the two types of experiments. Nevertheless, it is worth noting that the differences between the G values in compressive and tensile solicitation could be reasonably ascribed to the different behavior of the trapped water in the hydrogel samples relative to the two studied cases. A very interesting result of our work is that the relation of incompressibility ($E = 3G$) is verified to a good extent both in compression and in tensile experiments, even if they provide different values of the moduli in the two experimental setup [77].

Great interest is generally devoted to studies on the dynamic behavior of the material in the linear response regime and as a function of temperature. Therefore, a rheological study was carried out on the same pNIPAAM hydrogel after water equilibration: it candidates as new approach for the study of the swelling–deswelling transition as well as for inferring microscopic information on the physical properties of the material.

The main results of this investigation can be summarized as follows. We were able to monitor the equilibration of the material by recording the storage and loss moduli as a function of time, and we provided relaxation times of the material at different temperatures around the hydrogel phase transition temperature. It was not possible to reconstruct master curves by a shifting procedure of the frequency sweep shear modulus curves, suggesting that the hydrogel is behaving as a thermorheologically complex material.

Of particular relevance is the investigation of the equilibrium value of the storage shear modulus at 0.1 Hz as a function of temperature that allowed us to shed light on the swelling–deswelling transition region and to determine the transition temperature around 35 °C. Different thermal histories, pertinent to different heating/cooling rates for the hydrogel, evidenced the possibility of hysteresis in the temperature dependence of the shear modulus. These phenomena were interpreted starting from the relaxation time values of the hydrogel.

A relevant finding of our research was the correspondence of the shear modulus and the hydrogel volume as a function of temperature. This provided access to the thermal response of the polymer volume fraction ϕ_x, as a valuable parameter to describe the swelling–deswelling transition region exhibited by the pNIPAAM hydrogel. The experimental data of the polymer volume fraction were fitted with a phenomenological model, considering the transition as glass-type transition, and with different statistical models (CJF, phantom network, affine network, single chain and approximated single chain model). It was evidenced that our data could be successfully described by the CJF model, resulting from a mix of affine and phantom models of polymer networks.

Starting from these results, we were able to provide estimation for molar concentration of crosslinks, mesh size in the hydrogel and xerogel, as well as the average mass between crosslinks of pNIPAAM. In particular, the last result evidenced that the synthesis of the pNIPAAM hydrogel proceeded according to the stoichiometry of the materials.

As a final remark, the value of 0.4 kPa of the complex modulus G^* measured in the linear response regime at 25 °C provides a Young modulus of 1.2 kPa, under the assumptions of incompressibility, homogeneity and isotropy for the hydrogel. These values result being of one order of magnitude lower than those measured in the compressive and the tensile tests. This could be ascribed to the very different amounts of deformation applied in the rheological and mechanical experiments and to the fact that the incompressibility hypothesis is rather weak, given the role played by the water during the mechanical tests.

In conclusion, the joint analysis of both the mechanical response and the rheological behavior in the linear response regime represents a powerful investigation tool for the pNIPAAM hydrogel of the present work. This approach provides a good starting point for future investigations on different pNIPAAM hydrogel materials as well as an original paradigm for the study of complex systems.

Appendix A. Supplementary material

Supplementary data associated with this article can be found, in the online version, at http://dx.doi.org/10.1016/j.reactfunctpolym.2013.07.004.

References

[1] B.D. Ratner, A.S. Hoffman, Synthetic hydrogels for biomedical applications, in: J.D. Andrade (Ed.), Hydrogels for Medical and Related Applications, American Chemical Society, 1976, pp. 1–36.
[2] J.L. Drury, D.J. Mooney, Biomaterials 24 (2003) 4337–4351.
[3] D. Seliktar, Science 336 (2012) 1124–1128.
[4] O. Wichterle, D. Lim, Nature 185 (1960) 117–118.
[5] A. Gutowska, J. Seok Bark, I. Chan Kwon, Y. Han Bae, Y. Cha, S. Wan Kim, J. Control. Release 48 (1997) 141–148.
[6] S.-X. Cheng, J.-T. Zhang, R.-X. Zhuo, J. Biomed. Mater. Res. Part A 67A (2003) 96–103.
[7] D. Buenger, F. Topuz, J. Groll, Prog. Polym. Sci. 37 (2012) 1678–1719.
[8] K. Pal, A.K. Banthia, D.K. Majumdar, Des. Monomers Polym. 12 (2009) 197–220.
[9] H.G. Schild, Prog. Polym. Sci. 17 (1992) 163–249.
[10] R.V. Ulijn, N. Bibi, V. Jayawarna, P.D. Thornton, S.J. Todd, R.J. Mart, A.M. Smith, J.E. Gough, Mater. Today 10 (2007) 40–48.
[11] M.E. Harmon, D. Kuckling, C.W. Frank, Langmuir 19 (2003) 10660–10665.
[12] E.C. Muniz, G. Geuskens, Macromolecules 34 (2001) 4480–4484.
[13] A. Ikehata, H. Ushiki, Polymer 43 (2002) 2089–2094.
[14] T. Takigawa, T. Yamawaki, K. Takahashi, T. Masuda, Polym. Gels Networ. 5 (1998) 585–589.
[15] J. Zhang, R. Pelton, Y. Deng, Langmuir 11 (1995) 2301–2302.
[16] T. Sun, L. Feng, X. Gao, L. Jiang, Acc. Chem. Res. 38 (2005) 644–652.
[17] N. Gundogan, D. Melekaslan, O. Okay, Macromolecules 35 (2002) 5616–5622.
[18] A. Ikehata, M. Takano, H. Ushiki, Polym. J. 33 (2001) 554–559.
[19] T.R. Matzelle, G. Geuskens, N. Kruse, Macromolecules 36 (2003) 2926–2931.
[20] J.-T. Zhang, S.-W. Huang, S.-X. Cheng, R.-X. Zhuo, J. Polym. Sci., Part A: Polym. Chem. 42 (2004) 1249–1254.
[21] After the submission of the present work, we knew about a manuscript carried out in very different experimental conditions N. Adrus, M. Ulbricht, React. Funct. Polym. 73 (2013) 141–148.
[22] M.A. Stieger, W. Richtering, Macromolecules 36 (2003) 8811–8818.
[23] F. Zeng, X. Zheng, Z. Tong, Polymer 39 (1998) 1249–1251.
[24] M.V. Badiger, B.A. Wolf, Macromol. Chem. Phys. 204 (2003) 600–606.
[25] F.E. Antunes, L. Gentile, L. Tavano, C.O. Rossi, Appl. Rheol. 19 (2009) 42064–42072.
[26] C.A. DeForest, K.S. Anseth, Annu. Rev. Chem. Biomol. 3 (2012) 421–444.

[27] L. Yeghiazarian, H. Arora, V. Nistor, C. Montemagno, U. Wiesner, Soft Matter 3 (2007) 939–944.
[28] F. Horkay, G.B. McKenna, Polymer networks and gels, in: J.E. Mark (Ed.), Physical Properties of Polymers Handbook, Springer, 2007, pp. 497–523.
[29] J.-P. Pérez, Optique: Fondements et applications, seventh ed., Dunod, 2004.
[30] J.D. Jackson, Classical Electrodynamics, Wiley, 1998.
[31] F. Zulli, L. Andreozzi, E. Passaglia, S. Augier, M. Giordano, J. Appl. Polym. Sci. 127 (2013) 1423–1432.
[32] J.J. Aklonis, W.J. MacKnight, Introduction to Polymer Viscoelasticity, second ed., Wiley, 1983.
[33] I.M. Ward, D.W. Hadley, An Introduction to the Mechanical Properties of Solid Polymers, John Wiley & Sons, 1993.
[34] L.H. Sperling, Introduction to Physical Polymer Science, John Wiley & Sons, 1986.
[35] J.D. Ferry, Viscoelastic Properties of Polymers, third ed., John Wiley & Sons, 1980.
[36] G. Graf, S. Drescher, A. Meister, B. Dobner, A. Blume, J. Phys. Chem. B 115 (2011) 10478–10487.
[37] K.S. Anseth, C.N. Bowman, L. Brannon-Peppas, Biomaterials 17 (1996) 1647–1657.
[38] L.R.G. Treloar, The Physics of Rubber Elasticity, third ed., Oxford University Press, 2005.
[39] G.R. Strobl, The Physics of Polymers, third ed., Springer, 2007.
[40] M. Doi, S.F. Edwards, The Theory of Polymer Dynamics, Oxford University Press, 1988.
[41] I.I. Ward, J. Sweeney, Mechanical Properties of Solid Polymers, second ed., John Wiley & Sons, 2012.
[42] M.C. Boyce, E.M. Arruda, Rubber Chem. Technol. 73 (2000) 504–523.
[43] J.E. Mark, J. Chem. Educ. 58 (1981) 898–903.
[44] F. Bueche, Physical properties of polymers, Interscience Publishers, 1962.
[45] R.S. Rivlin, Philos. Trans. R. Soc. London, Ser. A 241 (1948) 379–397.
[46] P.J. Flory, Chem. Rev. 35 (1944) 51–75.
[47] N.R. Langley, Macromolecules 1 (1968) 348–352.
[48] L.M. Dossin, W.W. Graessley, Macromolecules 12 (1979) 123–130.
[49] D. Pearson, W. Graessley, Macromolecules 13 (1980) 1001–1009.
[50] W.W. Graessley, Adv. Polym. Sci. 47 (1982) 67–117.
[51] B. Erman, P.J. Flory, J. Chem. Phys. 68 (1978) 5363–5369.
[52] P.J. Flory, Principles of Polymer Chemistry, Cornell University Press, 1953.
[53] P.J. Flory, J.J. Rehner, J. Chem. Phys. 11 (1943) 521–526.
[54] J. Frenkel, Rubber Chem. Technol. 13 (1940) 264–274.
[55] A. Suzuki, M. Yamazaki, Y. Kobiki, J. Chem. Phys. 104 (1996) 1751–1757.
[56] A. Erbe, K. Tauer, R. Sigel, Phys. Rev. E 73 (2006) 031406.
[57] M. Reufer, P. Dıaz-Leyva, I. Lynch, F. Scheffold, Eur. Phys. J. E 28 (2009) 165–171.
[58] R.-S. Cheng, H. Yang, X.-H. Yan, W. Zhi-Liu, L. Li, Chem. J. Chinese Univ. 22 (2001) 1262–1264.
[59] J.C.M. Garnett, Philos. Trans. R. Soc. London, Ser. A 203 (1904) 385–420.
[60] M. Born, E. Wolf, Principles of Optics: electromagnetic Theory of Propagation, Interference and Diffraction of Light, Pergamon Press, 1980.
[61] X. Wang, X. Qiu, C. Wu, Macromolecules 31 (1998) 2972–2976.
[62] K. Takahashi, T. Takigawa, T. Masuda, J. Chem. Phys. 120 (2004) 2972–2979.
[63] P.G. De Gennes, Scaling Concepts in Polymer Physics, Cornell University Press, 1979.
[64] L. Andreozzi, M. Faetti, F. Zulli, M. Giordano, Macromolecules 37 (2004) 8010–8016.
[65] L. Andreozzi, M. Faetti, M. Giordano, D. Palazzuoli, F. Zulli, Macromolecules 36 (2003) 7379–7387.
[66] S. Sun, J. Hu, H. Tang, P. Wu, J. Phys. Chem. B 114 (2010) 9761–9770.
[67] C. Wu, Polymer 39 (1998) 4609–4619.
[68] M.L. Huggins, J. Am. Chem. Soc. 86 (1964) 3535–3540.
[69] F. Afroze, E. Nies, H. Berghmans, J. Mol. Struct. 554 (2000) 55–68.
[70] S. Cai, Z. Suo, J. Mech. Phys. Solids 59 (2011) 2259–2278.
[71] J.-P. Queslel, J.E. Mark, Swelling equilibrium studies of elastomeric network structures, Analysis/Reactions/Morphology, Springer, 1985.
[72] J.-P. Queslel, F. Fontaine, L. Monnerie, Polymer 29 (1988) 1086–1090.
[73] P.J. Flory, B. Erman, Macromolecules 15 (1982) 800–806.
[74] B. Erman, P.J. Flory, Macromolecules 15 (1982) 806–811.
[75] B. Erman, P.J. Flory, Macromolecules 16 (1983) 1601–1606.
[76] F. Zeng, Z. Tong, S. Takahiro, Science China Chemistry 42 (1999) 290–297.
[77] W.H. Han, F. Horka, G.B. Mckenna, Math. Mech. Solids 4 (1999) 139–167.